frontiers in Materials

ORIGINAL RESEARCH
published: 19 November 2019
doi: 10.3389/fmats.2019.00287

Effects of Curing Conditions on Shrinkage of Alkali-Activated High-MgO Swedish Slag Concrete

Abeer M. Humad[1,2]*, *John L. Provis*[3] *and Andrzej Cwirzen*[1]

[1] *Building Materials Group, Luleå University of Technology, Luleå, Sweden,* [2] *Civil Engineering Department, University of Babylon, Hillah, Iraq,* [3] *Department of Materials Science and Engineering, University of Sheffield, Sheffield, United Kingdom*

This study aimed to determine the effects of curing regime on shrinkage of alkali-activated concretes produced from a Swedish high-MgO blast furnace slag. Sodium carbonate (SC), sodium silicate (SS), and their combination were used as alkali activators. The studied curing procedure included heat-treatment, no heat-treatment, sealed and non-sealed conditions. The heat curing increased the compressive strengths of the concretes activated with SS and with the combination of SS and SC. Sealed-curing applied for a period of 1 month reduced the measured drying shrinkage by up to 50% for all studied heat-treated samples. Conversely, the same curing procedure significantly increased the development of the drying shrinkage once the seal was removed after 28 days of curing in the case of the SC-activated concretes non-heat treated. Higher degree of reaction/hydration reached by the binders in these concretes was indicated as the main factor. All of the concretes studied had showed a significant microcracking of the binder matrix, with the most extensive cracking observed in the sealed lab-cured mixes. The heat-cured mixes activated with SS and combination of SC and SS showed the most homogenous microstructure and low extensive micro cracking comparing with lab-cured ones.

Keywords: Alkali activated slag concrete, microstructure, drying shrinkage, curing regime, high MgO granulated blast furnace slag

OPEN ACCESS

Edited by:
Xiangming Zhou,
Brunel University London,
United Kingdom

Reviewed by:
Sriramya Duddukuri Nair,
Cornell University, United States
Fei Jin,
University of Glasgow,
United Kingdom

***Correspondence:**
Abeer M. Humad
abeer.humad@ltu.se;
abeer_alasady@yahoo.com

Specialty section:
This article was submitted to Structural Materials, a section of the journal Frontiers in Materials

Received: *19 May 2019*
Accepted: *29 October 2019*
Published: *19 November 2019*

Citation:
Humad AM, Provis JL and Cwirzen A (2019) Effects of Curing Conditions on Shrinkage of Alkali-Activated High-MgO Swedish Slag Concrete. Front. Mater. 6:287. doi: 10.3389/fmats.2019.00287

INTRODUCTION

Granulated blast furnace slag (GBFS) is a by-product derived from the iron-making process, and is quenched from its molten state to form an amorphous material consisting mainly of a calcium-magnesium aluminosilicate glass. Ground GBFS is also widely used as a supplementary cementitious material in Portland cement—based systems (PC), to lower the hydration heat and to improve the chemical durability of concrete, especially in acid exposures (Chidiac and Panesar, 2008). The use of the alkali-activated slag (AAS) binders to produce concretes enabled up to 75% reduction of the carbon emissions footprint in comparison with plain Portland cement (Yang et al., 2013).

The mechanical properties of AAS concretes are controlled by physical properties and chemical composition of the used slag precursor, the activator type and its dose, curing temperature but also a number of other parameters (Atiş et al., 2009; Bernal et al., 2014a; Myers et al., 2017; Criado et al., 2018). The most commonly used alkali activators include; sodium hydroxide, sodium silicate, sodium sulfate, and sodium carbonate (Provis and Van Deventer, 2014; Criado et al., 2018).

The setting times of AAS pastes activated by sodium silicate and sodium carbonate were found to be significantly longer than that of the OPC. On the other hand, slag paste activated with sodium carbonate had similar setting behavior as the PC-based concretes (Atiş et al., 2009).

AAS concretes showed good resistance to acid attack, fire exposure and corrosion (Jiang et al., 1997; Chidiac and Panesar, 2008; Karahan and Yakupoglu, 2011; Mundra et al., 2017). Most AAS concretes activated by sodium silicate or sodium hydroxide showed higher early and flexural strength (Bakharev et al., 1999), but they are more sensitive to the curing temperature than PC. The apparent activation energy is higher but it develops lower hydration heat and faster reaction rates (Shi and Day, 1996; Shi et al., 2006; Aydin and Baradan, 2012; Provis et al., 2015).

In general AAS develop higher shrinkage in comparison with PC concretes (Allahverdi et al., 2017; Humad et al., 2018; Orosz et al., 2019). In the case of the SS activated GGBFS concretes, the high shrinkage was linked with the presence of more mesopores (Shi, 1996) which led to the increased tensile stresses and thus to a greater drying shrinkage (Häkkinen, 1993). SS-activated slag mortars developed up to six times higher drying shrinkage in comparison with mortars based on PC mortars (Atiş et al., 2009). Conversely, SC-activated slag showed lower or equal drying shrinkage values in comparison with PC based systems. The shrinkage kinetics appeared to be slower at a similar RH (Zheng, 2010; Ye and Radlinska, 2016). The hydration products of the AAS included C-S-H gel with a lower Ca/Si ratio than that in PC, with a Si-rich gel, containing higher amount of un-combined water content. This un-combined water would evaporate during the drying process, subsequently causing a significant shrinkage (Collins and Sanjayan, 2000; Ye and Radlinska, 2016; Ye et al., 2017). Shrinkage of the ASC is strongly influenced by the applied curing conditions. For example exposure to the relative humidity (RH) between 50 and 70% was indicated as especially unfavorable (Douglas et al., 1992; Bakharev et al., 1999; Krizan and Zivanovic, 2002; Provis and Van Deventer, 2014; Ye et al., 2017). A partial replacement of BFS with FA tended to lower the drying shrinkage (Wallah and Rangan, 2006; Singh et al., 2016; Humad et al., 2019). Decrease of the NaO to SiO_2 molar ratio of the SS alkali activation reduced the drying shrinkage values, but increased the autogenous shrinkage (Krizan and Zivanovic, 2002; Atiş et al., 2009; Humad et al., 2019).

Heat treatment can significantly accelerate the strength development of AAS concrete, and has been observed to reduce the ultimate shrinkage values in comparison with the PC concrete (Bakharev et al., 1999). The heat curing resulted in a coarser porosity and thus decreased drying shrinkage (Bakharev et al., 2000; Ismail et al., 2013). A similar effect was observed while using shrinkage reducing admixtures (SRA). In that case, the drying shrinkage was reduced by formation of a coarser pore structure which led to the reduction of the pore fluid surface tension (Palacios and Puertas, 2007).

The high MgO content GGBFS, which is the focus of the research results presented in this publication, can be found only in few locations around the world. Sweden is one example where all locally produced GGBFS has MgO content between 12 and 19-wt.%. Previous studies showed that the reaction chemistry and the developed microstructure are remarkably altered in those systems with a possible strong effect on shrinkage. The incorporation of Al in the C-S-H type gel which is typical for AAS systems was reduced at a high BFS MgO content. The available Al was strongly consumed through the formation of hydrotalcite-group minerals (Ben Haha et al., 2011). An increase of the MgO content in AAS systems activated by SS, enhanced the formation of hydrotalcite and formed a more disordered silicate gel microstructure (Ben Haha et al., 2011; Bernal et al., 2014b). Increasing the MgO content in alkali-activated slag system showed increased carbonation resistance (Bernal et al., 2014b; Park et al., 2018).

The problem of an excessive drying shrinkage in AAS concrete is known and has been studied well relatively for binder systems based on commonly available low MgO content blast furnace slags. On the contrary, the amount of the available data related to AAS based on high MgO content BFS is rather limited. The present research aimed to fill in this lack of knowledge and focused on effects of various curing conditions, mechanical properties, and microstructure on shrinkage of a typical high MgO blast furnace slag available in Sweden on the development of drying and autogenous shrinkage.

MATERIALS AND METHODS

A (GBFS), type Merit 5000 (MEROX, Sweden), was used as a main binder in this study. Its chemical composition determined using a PANalytical-Zetium XRF spectrometer is shown in **Table 1**. The physical properties were provided by the supplier, Sodium carbonate and sodium silicate were used as alkali activators. The powdered sodium carbonate (SC) was provided by CEICH SA from Poland while the liquid sodium silicate (SS) by the PQ Corporation. The SS as supplied had the alkali modulus (M_s = mass ratio SiO_2/Na_2O) of = 2.2, with 34.37 wt.% SiO_2, 15.6 wt.% Na_2O and solids content of 49.97 wt.%. The M_s value was adjusted to 1.0 by addition of sodium hydroxide pellets (98% purity), with 76.31 wt.% Na_2O. The alkali activator dosage varied between 5 and 10 wt.% of the total binder content, **Table 2**. The BFS content in all concrete mixes was 450 kg/m^3, and the total water to binder (w/b) ratio was 0.45. Jehander group from Sweden provided coarse granite aggregates (size 4–8 mm) and fine aggregates which grading curves are shown in **Figure 1**. The fine aggregate content in the concrete mix was about 80 wt.% of the total aggregate amount. Liquid sodium silicate and powder sodium carbonate were dissolved in the mixing water 24 h before production of concrete. All dry ingredients including GBFS, coarse and fine aggregates were mixed for 1 min followed by an addition of the mixing water containing alkali activators and mixed for another 3 min. A rotating pan mixer type Zyklos-ZZ75HE was used to prepare all the mixes.

Initial and final setting times were determined using the Vicat apparatus, following the ASTM C191-13 standard. Flexural strength was determined on 28-day old beams of 100 × 100 × 500 mm^3, in three point bending following the SS-EN 12390-5:2009 standard. The applied load rate was 160 N/sec. 7 and 28-days compressive strengths were determined as average values from

TABLE 1 | Details of GGBFS used in this work.

Component	CaO	SiO_2	Al_2O_3	Fe_2O_3	MgO	Na_2O	K_2O	TiO_2	MnO	SO_3	L.O.I
Composition represented as oxides wt.%	30.4	35	14.3	0.3	16.1	0.6	0.7	2.8	0.5	0.7	0.9
Physical data	Specific surface(cm^2/g)			Bulk density (kg/m^3)				Particle density (kg/m^3)			
	5,000			1,100				2,950			

TABLE 2 | Mix proportions of concretes.

Mix ID	Binder (GBFS) content kg/m^3	Total w/b ratio	Aggregate content (0–8 mm) kg/m^3	Activator type, % dosage as solid materials	Curing condition	pH value of the activator solution	Slump results in mm
SC10L	450	0.45	1,663	10% SC	Lab curing	11.2	80
SC10H	450	0.45	1,663	10% SC	Heat curing		
SS10L	450	0.45	1,663	10% SS, M_s =1	Lab curing	13.7	250
SS10H	450	0.45	1,663	10% SS, M_s =1	Heat curing		
SC5 + SS5L	450	0.45	1,663	5% SC+5% SS	Lab curing	13.3	180
SC5 + SS5H	450	0.45	1,663	5% SC+5% SS	Heat curing		

SS, sodium silicate; SC, sodium carbonate; L suffix after mix refers to laboratory-cured mix; H suffix after mix refers to heat-cured mix.

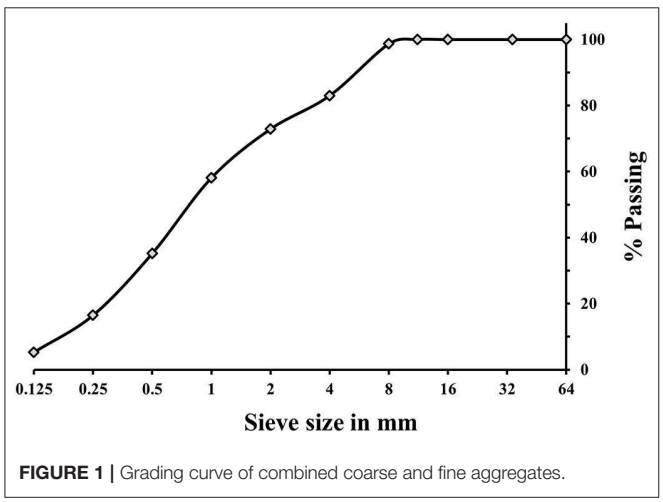

FIGURE 1 | Grading curve of combined coarse and fine aggregates.

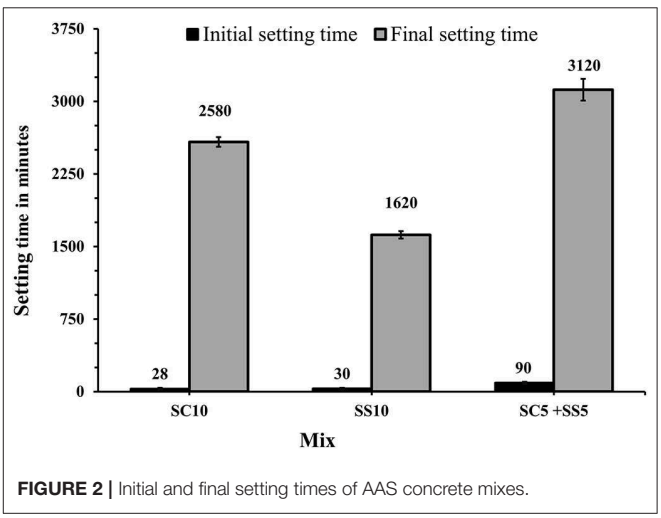

FIGURE 2 | Initial and final setting times of AAS concrete mixes.

three tests on 100 × 100 × 100 mm^3 cubes following the SS-EN 12390-3 standard. The loading rate was set to 10 KN/s.

Shrinkage was determined using cylinders having a diameter of 100 mm and a height of 200 mm. The shrinkage measurements started 1.5 days after casting for the heat-cured sample and after 2–3 days for the laboratory-cured samples, depending on the measured final setting time, **Figure 2**. All samples were subsequently stored in laboratory conditions. Strain values were recorded using a strain gauge DEMEC type product by Mayes Instruments Limited. Two pairs of stainless steel measuring discs were glued with an epoxy resin onto each cylinder and were spaced at 100 mm apart.

The curing procedure applied to samples used for the determination of the compressive and flexural strength tests included sealing with plastic bags followed by storage of the specimens in the laboratory conditions at 20 ± 2°C and 40 ± 3% RH until testing. The second procedure included heat curing at 65°C for 24 h applied immediately after casting followed by a storage in the laboratory at 20 ± 2°C and 40 ± 3% RH. Samples used for shrinkage tests determination were subjected to two additional curing procedures, **Table 3**. The third procedure included sealing only for 2–3 days after hardening. After seal removal samples were stored at 20 ± 2°C and 40 ± 3% RH (L unsealed), **Table 3**. Heat curing of sealed samples at 65°C for 24 h was applied in the 4th variant and was followed by removal of the seal and storage of the specimens in the laboratory conditions at 20 ± 2°C and 40 ± 3% RH (H unsealed).

"Microstructure and microchemistry of hardened samples were studied using scanning electron microscope (SEM) model JSM-IT100 combined with a QUANTAX EDX (Energy-dispersive X-ray spectroscopy) analysis system from BRUKER and the ESPRIT 2 software. Concrete samples for the SEM analysis were cut from 28-days old specimens. Moisture was moved

TABLE 3 | Curing details symbols of lab- and heat-cured samples of shrinkage measurement.

Mix ID	Lab- or heat-cured samples sealed for 1 month	Lab- or heat-cured samples opened after hardened
SC10 L	SC10 L sealed	SC10 L unsealed
SC10 H	SC10 H sealed	SC10 H unsealed
SS10 L	SS10 L sealed	SS10 L unsealed
SS10 H	SS10 H sealed	SS10 H unsealed
SC5 + SS5 L	SC5 + SS5 L sealed	SC5 + SS5 L unsealed
SC5 + SS5 H	SC5 + SS5 H sealed	SC5 + SS5 H unsealed

SS, sodium silicate; SC, sodium carbonate; L sealed suffix after mix refers to laboratory-cured mix sealed for 1 month; H unsealed suffix after mix refers to heat-cured mix opened after hardening.

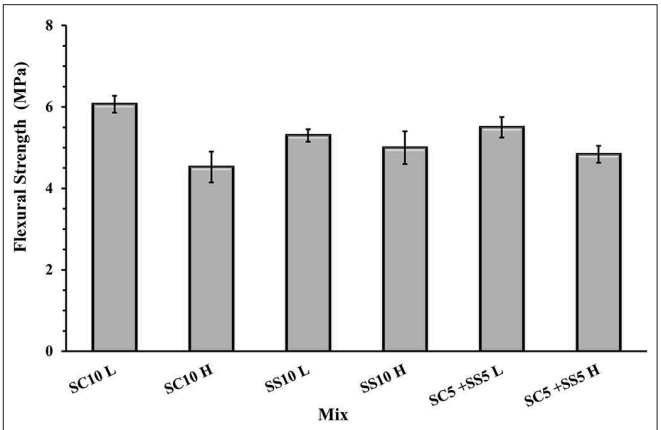

FIGURE 3 | Flexural test results of concrete beams after 28 days of sealed curing.

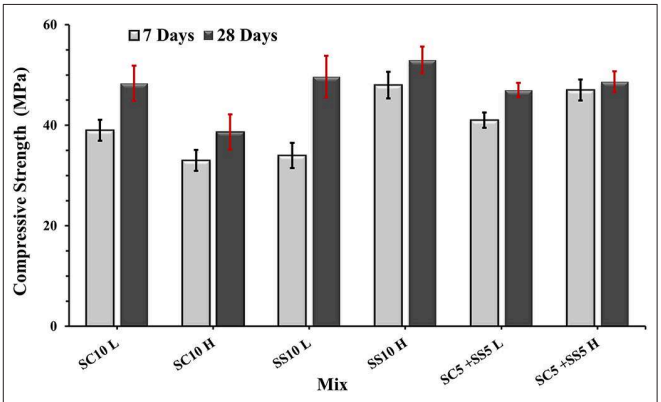

FIGURE 4 | Compressive strength test results of concrete cubes after 7 and 28 days of sealed curing.

from all specimens using an alcohol exchange techniques where sample were stored in alcohol for 48 h. In the following step, specimens were moved to the low vacuum impregnation chamber and impregnated with low viscosity resin. No heat drying of the samples was applied to maximally limit formation of microcracks. After curing for 24 h resin impregnated samples were grinded and polished in steps using polishing spray containing 9, 3, and 1 μm synthetic diamond particles. During polish a load of 35 N was applied in the polishing head. The SEM was operating at using 15.0 kV accelerating voltage and probe current of 61–72 mA."

RESULTS AND DISCUSSION

The shortest initial setting times were measured for mixes activated with 10 wt.% of SC and 10 wt.% of SS (SC10, SS10, respectively). The longest final setting times were observed for mixes activated with 10 wt.% SC and the combination of 5 wt.% of SC + 5 wt.% of SS (SC10, SC5 + SS5), **Figure 2**. These results can be explained by a high concentration of calcium carbonate and high MgO content which resulted in formation of gaylussite, hydrotalcite and calcite (Humad et al., 2018). Earlier studies showed that a presence of calcite $CaCO_3$ tends to shorten the initial setting time rapidly and decreases the viscosity of the fresh mix. At the same time, it extended the final setting due to slower reaction rates and a longer induction period. The pH values of those systems were also observed to be significantly lower, (Sariibrahimoglu et al., 2012; Provis and Van Deventer, 2014; Bernal, 2016).

The flexural strength of the AAS concrete beams reached between 4.5 and 6.0 MPa with slightly lower values for the heat-cured samples, **Figure 3**. The highest 7- and 28-day compressive strength was measured for the heat-treated samples activated with 10 wt.% SS, while the lowest for the heat-cured sample activated with 10 wt.% SC (mix SC10 H), **Figure 4**. There is no evident correlation between compressive and flexural strength among tested samples. Few mixes had relatively high compressive strengths but showed lower flexural strengths, which could be related to microcracking of the binder matrix. Similar trends were also observed by others in the PC based systems (Wedatalla et al., 2019). The chemical composition and particles size distribution strongly affects the kinetics reaction and the evolution of solid structural phases forming in alkali-activated slag (AAS) system. At high MgO contents (MgO > 5%), the hydrotalcite phases and the C–(N)–A–S–H type gels were observed to be formed (Bernal et al., 2014b). The lowered Al uptake by the C-S-H resulted in an increased 28-days compressive strength. An increasing MgO content of SH- and SS-activated slag pastes showed more rapid strength development and higher compressive strength at early and late hydration times (Ben Haha et al., 2011). The highest increase of the compressive strength between 7 and 28 days was observed for the non-heat-treated samples activated with 10 wt.% SS (mix SS10 L) while the lowest for the heat-treated samples activated with 5 wt.% SC and 5 wt.% SS (mix SC5 + SS5 H). A lack of the moisture required to continue the reaction of GBFS could be indicated as one of the possible reasons (Collins and Sanjayan, 2001). Higher initial hydration/reaction rate observed in heat-cured mixes followed by its significant slowdown can be also related to the formation of a dense impermeable binder matrix surrounding the unreacted particles. The efficient amount of available GBFS will be limited. The formed binder matrix will

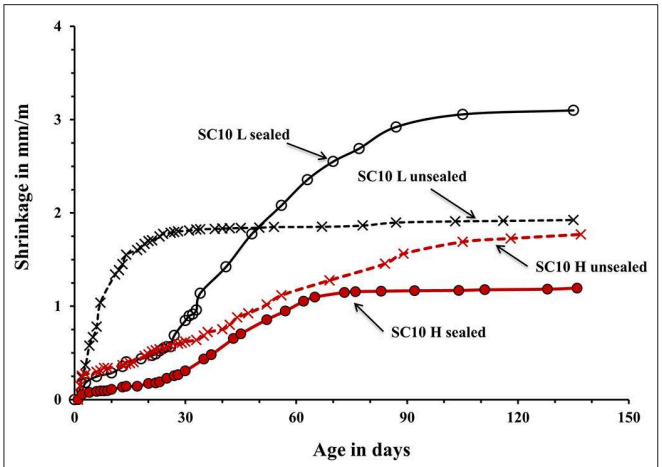

FIGURE 5 | Shrinkage of the laboratory- and heat-cured AAS concrete samples activated by 10% sodium carbonate SC.

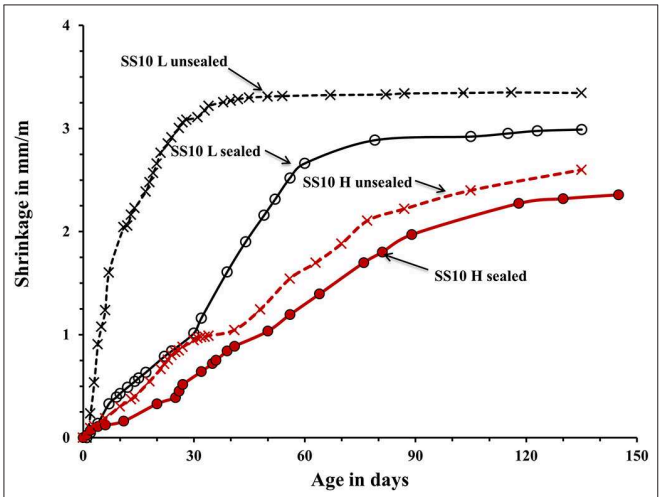

FIGURE 6 | Shrinkage of the laboratory- and heat-cured AAS concrete samples activated by 10% sodium silicate SS.

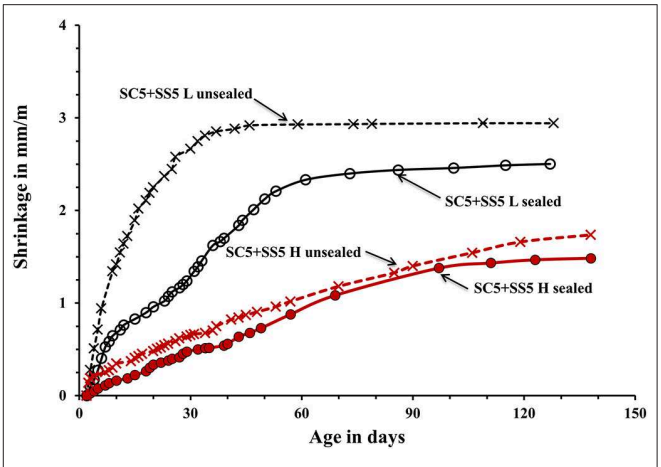

FIGURE 7 | Shrinkage of the laboratory- and heat-cured AAS concrete samples activated by 5% SC + 5% SS.

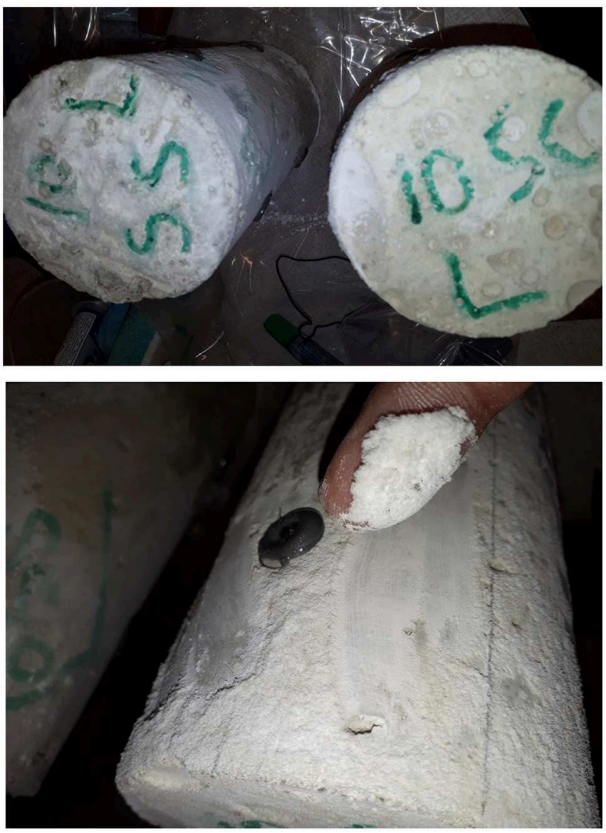

FIGURE 8 | SEM-BSE images of fragments of 28 days (sealed) AAS concrete samples show the microcracking which filled with resin.The right side shows the lab-cured samples (marked L), and the left side shows the heat-cured samples (marked H). Agg., aggregate particle; BFS, unreacted or partially reacted blast furnace slag particle. The scale bar in each image represents 50 μm.

be also less homogenous with larger amount of pores (Helmuth and Verbeck, 1968; Shi et al., 2006).

The used curing procedure aimed to simulate real life conditions where sufficient control is only possible for a limited amount of time. The main difference between the sealed and unsealed samples was the ultimate contribution of the autogenous and drying shrinkage. The sealed curing hindered the development of the drying shrinkage and produced a strong and dense binder matrix able to resist volumetric changes without extensive microcracking. Contrary, the used unsealed curing enabled a development of both types of shrinkage. The measured shrinkage values are shown in **Figures 5**–**7**. In general, concretes activated with the sodium carbonate, had a significantly lower shrinkage in comparison with mixes activated with the sodium silicate. The lowest shrinkage of 1.1 mm/m was measured on SC-activated slag concrete (mix SC10 H sealed) subjected to the heat-treatment, which was followed by one-month curing in sealed conditions, **Figure 5**. Mixes activated with 10 wt.% SS and 5 wt.% SC + 5 wt.% SS, subjected to the same curing procedure developed 2.4 and 1.5 mm/m of shrinkage, respectively. Those higher values can be related to more intensive chemical reactions

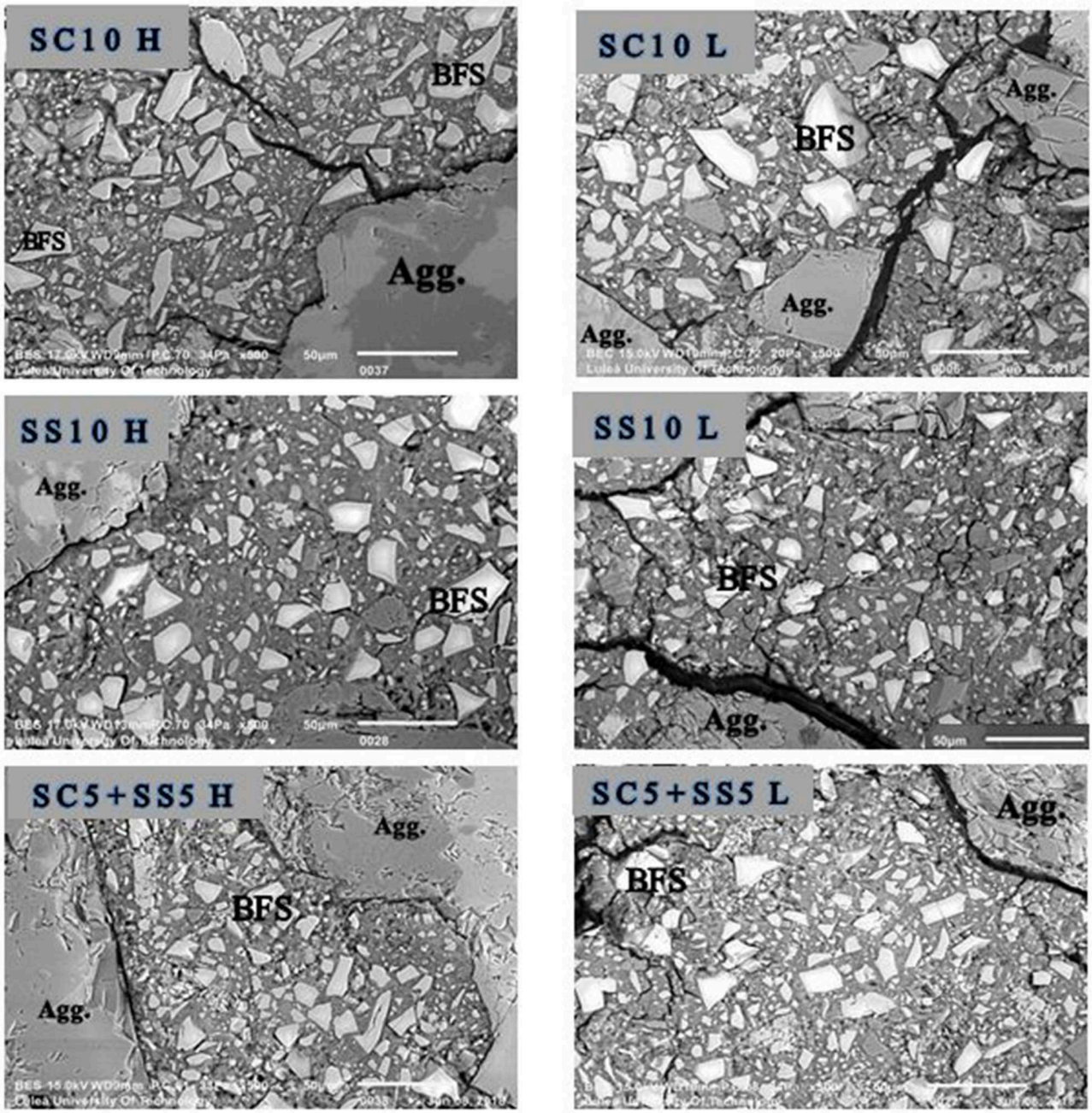

FIGURE 9 | Efflorescence of lab-cured samples when de-molded at early age and left open in a laboratory environment for 2–3 h.

triggered by a high pH values. The formed microstructure was finer presumably also leading to intensive self-desiccation as observed by others (Zhang et al., 2013; Mosale Vijayakumar, 2014). The number of empty pores most probably increased due to more intensive reactions which eventually resulted in a higher shrinkage (Neto et al., 2008).

The applied heat treatment decreased the measured shrinkage. In the case of mixes activated with a combination of 5 wt.% SC + 5 wt.% SS the maximum reduction reached 41%. The heat treatment presumably produced coarser microstructure of the binder matrix which lead to lower tensile strains induced by the evaporation of the pore water and lower shrinkage values (Bakharev et al., 2000; Collins and Sanjayan, 2000; Ismail et al., 2013). As described earlier, a higher curing temperature most probably lead to a more intensive formation of reaction products around slag particles thus limiting or fully inhibiting its further dissolution which provides all required for the solidification reaction species (Bakharev et al., 1999). The heat-cured samples

showed only a moderate enhancement of the measure ultimate compressive strength, which further supports that mechanism. A similar effect of the high curing temperature was observed in Portland cement based concretes (Helmuth and Verbeck, 1968). A significant and unfortunately, unmeasured proportion of the shrinkage developed already during the heat treatment. The application of the 1-month sealed-curing reduced the measured shrinkage by up to 61% in the case of concretes activated with 10-wt.% SC, **Figure 5**. A combination of the heat treatment and the 1 month sealed curing reduced the measured shrinkage by up to 50% for the mix SC5 + SS5, **Figure 7**. The sealed curing presumably additionally increased the tensile strength of the binder matrix and decreased its carbonation (Ma and Dehn, 2017).

The SEM-BSE analysis showed an intensive microcracking of the binder matrix. In the analysis of the obtained images only cracks filled with resin were considered which excluded crack, which could form due to vacuum conditions present in the SEM specimen chamber. In general, the microcracking was more extensive in non-heat-treated samples, which can be related with the high early age shrinkage, **Figure 8**. Conversely, the heat-cured samples showed less microcracking, especially the mixes SS10 H and SC5 + SS5 H due to stronger matrix and coarser microstructure.

Efflorescence was observed in non-heat-treated samples during de-molding, **Figure 9**. The phenomenon was caused by a migration of sodium hydroxide from the pore solution to the surface of samples during drying and its subsequent reaction with atmospheric carbon dioxide. As a results the sodium carbonate was formed (Higgins, 1982). The hydroxide remains water-soluble only for a short period after the exposure to the atmosphere as it reacts with CO_2 to form carbonate salts (Higgins, 1982). The observed strong tendency of AAS binders toward the efflorescence can be related to the high alkali concentration in the pore solution. In certain alkali activated concretes, this can be exaggerated by an open microstructure caused by for example a lower reaction degree, and a weak exchangeable binding of Na (Wang et al., 1995; Lloyd et al., 2010; Allahverdi et al., 2017; Longhi et al., 2019). Earlier studies showed that in SC-activated binders, calcium and sodium-calcium carbonates tend to form at early stages rather than the strength-defining C-A-S-H phases (Fernández-Jiménez et al., 2003). After 28 days, a highly cross-linked C-A-S-H providing a higher strength phase was reported to form (Fernández-Jiménez et al., 2003; Xu et al., 2008).

The high MgO content of the slag tends to affect the early-age properties of the binder matrix. Earlier studies, also performed by the authors, indicated formation of hydrotalcite-like Mg-Al layered double hydroxides (Bernal et al., 2016; Humad et al., 2018; Abdollahnejad et al., 2019). The consumption of Al may also contribute to the strength development. The phase composition at each age can be controlled by the consumption of CO_3^{2-} species from the activator. For example, calcium carbonates are formed using Ca^{2+} released from the GBFS. Carbonates can be up taken by the Mg–Al layered double hydroxide phases. When the CO_3^{2-} species are consumed, the pH will increase and the reaction is believed to continue similarly as in the case of binders activated with sodium hydroxide (Xu et al., 2008; Bernal et al., 2015). In the present study, the applied heat curing (at 65°C) affected the dissolution process of the GBFS, and thus also the availability of Ca^{2+} and CO_3^{2-} at the early age. Although, not verified experimentally, it is very likely that the dissolution rate of GBFS was higher in the heat-cured samples thus leading to a more intensive formation of calcite and gaylussite. The formation of gaylussite was shown earlier to be predominant at an early age, in high-MgO AAS binders (Humad et al., 2018). The high sodium carbonate content in the mix SC10 provided an excess of Na ions, which supported the formation of gaylussite $Na_2Ca(CO_3)_2{\cdot}5H_2O$ (Allahverdi et al., 2017). In the next stage, the gaylussite started to dissolve and changed to more stable phases besides the formation of C-A-S-H was initiated (Allahverdi et al., 2017; Humad et al., 2018).

The results from the SEM-EDX analysis are shown in the form of ternary diagrams; CaO, Al_2O_3 and SiO_2, **Figure 10**.

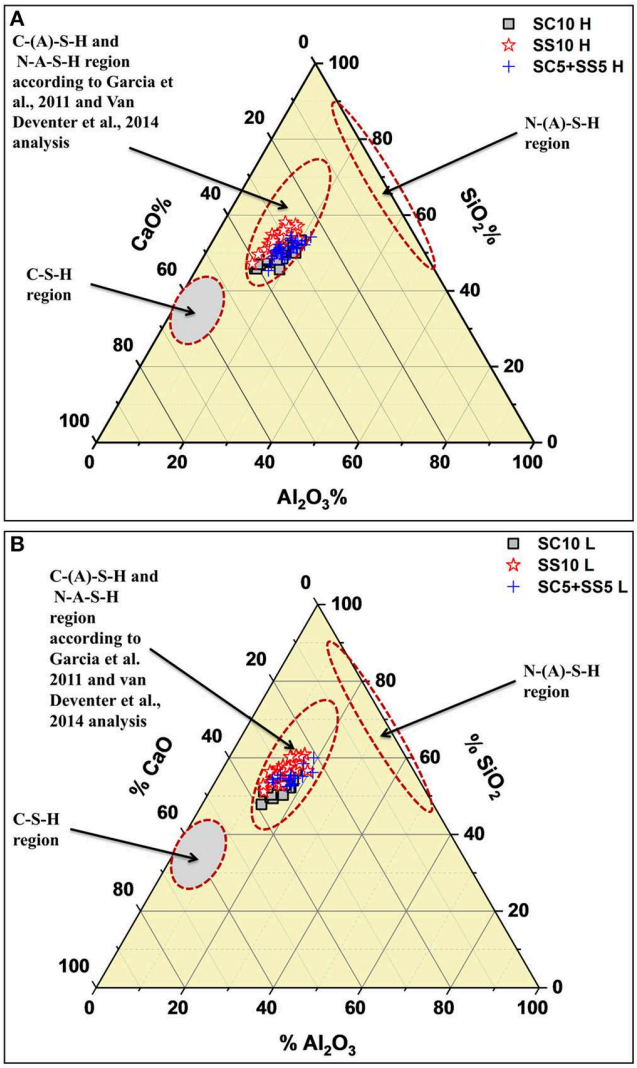

FIGURE 10 | Ternary diagrams showing the oxide composition regions of the sealed AAS concretes (28 days old) measured with SEM/EDX and compared with (Garcia-Lodeiro et al., 2011; Van Deventer et al., 2014) results; **(A)** for heat-cured samples, **(B)** for lab-cured samples.

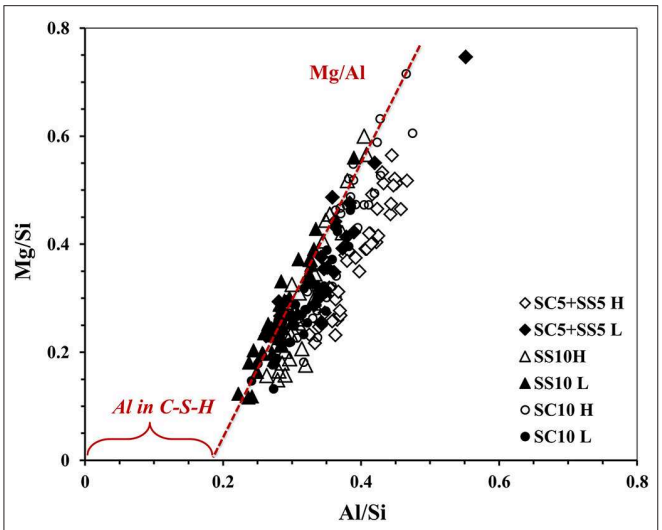

FIGURE 11 | EDX analysis results after 28-day, show atomic ratio Al/Si vs. Mg/Si of AAS concrete, heat, and lab-cured.

Based on earlier studies typical regions for CSH, N(A)-S-H and C(A)-S-H are marked (Garcia-Lodeiro et al., 2011; Van Deventer et al., 2014). The values obtained from spot analyses of the binder matrix appeared to be located in the area predominantly assigned to C(A)-S-H phase, thus further supporting earlier formulated conclusion. Furthermore, higher amounts of SiO_2 and lower amounts of calcium were detected in the laboratory cured samples, **Figure 10A**. It could be related to a lower degree of reaction/hydration similarly as in the case of the Portland cement based systems (Helmuth and Verbeck, 1968).

The amount of Al up takes in C-S-H could be predicted from **Figure 11**, where all the mixes displayed overlapping at the same area. The presence of a positive value in x-axis in the Al/Si vs. Mg/Si ratios indicates the formation of a hydrotalcite-like phase and the presence of Al in the C-S-H (Ben Haha et al., 2011), with Mg/Al ratio of 1.1, 0.91, and 0.94 for mixes SC10 H, SS10 H and SC5 + SS5 H, respectively. While for lab-cured samples the Mg/Al ratios were 0.88, 0.89 and 1.06 for mixes SC10 L, SS10 L and SC5 + SS5 L respectively. However, the Al incorporation in C-S-H decreased with increased MgO content. Ben Haha et al. (2012) stated that the hydrotalcite-like phases formed during the first days having an Mg/Al ratio of ∼2, then declines with time at later age to be 1.3 or even 0.5, which means poor hydrotalcite was presented in all mixes of this study, **Figure 11**.

CONCLUSIONS

High MgO content Swedish GGBFS was studied to determine effects of curing conditions on the development of shrinkage of alkali activated concretes. Additionally, setting times, microstructure, chemical composition and compressive strength were determined as well. Four different curing procedures were evaluated including heat-treatment and no-heat-treatment in combination with sealed and unsealed conditions. The obtained results confirmed that all measured parameters were affected by the applied curing procedure. The non-heat treated sealed-cured samples produced higher 28-day compressive strengths when activated with sodium carbonate. The application of the heat treatment combined with the sealed-curing for those concretes resulted in lower strengths. All non-heat-treated and unsealed samples showed higher shrinkage, while the application of the combined heat-treatment and sealed-curing reduced these values by 30–50%. The reduction was related to the development of more intensive hydration/geopolymerization reaction leading to a denser binder matrix having a higher tensional strength. Consequently, the drying and carbonation shrinkage were reduced by sealing. The heat-treated samples showed less micro-cracked and coarser microstructure additionally indicating higher tensional strength of the binder matrix.

All presented results are based only one high MgO BFS which limits to formulate generalized concussions. Therefore, the future research should focus on testing slags with variable amounts of MgO.

DATA AVAILABILITY STATEMENT

All datasets generated for this study are included in the article/supplementary material.

AUTHOR CONTRIBUTIONS

AH: did all tests, organized the database, performed the statistical analysis, and wrote the first draft of the manuscript. JP and AC: revision read and approved the submitted version.

ACKNOWLEDGMENTS

The Iraqi Ministry of Higher Education and Scientific Research, Iraq, and Luleå University of Technology LTU, Sweden financed this research. The authors would like to thank the technical staff of the MCE laboratory at LTU, Sweden.

REFERENCES

Abdollahnejad, Z., Luukkonen, T., Mastali, M., Yliniemi, J., Kinnunen, P., and Illikainen, M. (2019). "Development of alkali-activated magnesium aluminosilicate binders from soapstone," in *Proceedings of the International Conference on Sustainable Materials, Systems and Structures, New Generation of Construction Materials, RILEM Proceedings PRO 128* (Rovinj-Croatia). 337–344.

Allahverdi, A., Kani, E. N., and Shaverdi, B. (2017). Carbonation versus efflorescence in alkali-activated blast-furnace slag in relation with chemical composition of activator. *Int. J. Civil Eng.* 15, 565–573. doi: 10.1007/s40999-017-0225-4

Atiş, C. D., Bilim, C., Çelik, Ö., and Karahan, O. (2009). Influence of activator on the strength and drying shrinkage of alkali-activated slag mortar. *Constr. Build. Mater.* 23, 548–555. doi: 10.1016/j.conbuildmat.2007.10.011

Aydin, S., and Baradan, B. (2012). Mechanical and microstructural properties of heat cured alkali-activated slag mortars. *Mater. Design.* 35, 374–383. doi: 10.1016/j.matdes.2011.10.005

Bakharev, T., Sanjayan, J., and Cheng, Y. (1999). Effect of elevated temperature curing on properties of alkali-activated slag concrete. *Cement Concrete Res.* 29, 1619–1625. doi: 10.1016/S0008-8846(99)00143-X

Bakharev, T., Sanjayan, J., and Cheng, Y. (2000). Effect of admixtures on properties of alkali-activated slag concrete. *Cement Concrete Res.* 30, 1367–1374. doi: 10.1016/S0008-8846(00)00349-5

Ben Haha, M., Lothenbach, B., Le Saout, G., and Winnefeld, F. (2011). Influence of slag chemistry on the hydration of alkali-activated blast-furnace slag—Part I: effect of MgO. *Cement Concrete Res.* 41, 955–963. doi: 10.1016/j.cemconres.2011.05.002

Ben Haha, M., Lothenbach, B., Le Saout, G., and Winnefeld, F. (2012) Influence of slag chemistry on the hydration of alkali-activated blast-furnace slag - Part II: effect of Al_2O_3. *Cement Concrete Res.* 42, 74–83. doi: 10.1016/j.cemconres.2011.08.005

Bernal, S. A. (2016). Advances in near-neutral salts activation of blast furnace slags. *RILEM Tech. Lett.* 1, 39–44. doi: 10.21809/rilemtechlett.2016.8

Bernal, S. A., Provis, J. L., Fernández-Jiménez, A., Krivenko, P. V., Kavalerova, E., Palacios, M., et al. (2014a). "Binder chemistry–high-calcium alkali-activated materials," in *Alkali Activated Materials*, ed J. Provis (Sheffield: Springer), 59–91.

Bernal, S. A., Provis, J. L., Myers, R. J., San Nicolas, R., and van Deventer, J. S. (2015). Role of carbonates in the chemical evolution of sodium carbonate-activated slag binders. *Mater. Struct.* 48, 517–529. doi: 10.1617/s11527-014-0412-6

Bernal, S. A., San Nicolas, R., Myers, R. J., De Gutiérrez, R. M., Puertas, F., Van Deventer, J. S., et al. (2014b). MgO content of slag controls phase evolution and structural changes induced by accelerated carbonation in alkali-activated binders. *Cement Concrete Res.* 57, 33–43. doi: 10.1016/j.cemconres.2013.12.003

Bernal, S. A., San Nicolas, R., van Deventer, J. S., and Provis, J. L. (2016). Alkali-activated slag cements produced with a blended sodium carbonate/sodium silicate activator. *Adv. Cem. Res.* 28, 262–273. doi: 10.1680/jadcr.15.00013

Chidiac, S., and Panesar, D. (2008). Evolution of mechanical properties of concrete containing ground granulated blast furnace slag and effects on the scaling resistance test at 28 days. *Cement Concrete Composites* 30, 63–71. doi: 10.1016/j.cemconcomp.2007.09.003

Collins, F., and Sanjayan, J. (2000). Effect of pore size distribution on drying shrinking of alkali-activated slag concrete. *Cement Concrete Res.* 30, 1401–1406. doi: 10.1016/S0008-8846(00)00327-6

Collins, F., and Sanjayan, J. G. (2001). Microcracking and strength development of alkali activated slag concrete. *Cement Concrete Compos.* 23, 345–352. doi: 10.1016/S0958-9465(01)00003-8

Criado, M., Walkley, B., Ke, X., Provis, J., and Bernal, S. (2018). Slag and activator chemistry control the reaction kinetics of sodium metasilicate-activated slag cements. *Sustainability* 10:4709. doi: 10.3390/su10124709

Douglas, E., Bilodeau, A., and Malhotra, V. (1992). Properties and durability of alkali-activated slag concrete. *ACI Mater. J.* 89, 509–516. doi: 10.14359/1832

Fernández-Jiménez, A., Puertas, F., Sobrados, I., and Sanz, J. (2003). Structure of calcium silicate hydrates formed in alkaline-activated slag: Influence of the type of alkaline activator. *J. Am. Ceramic Soc.* 86, 1389–1394. doi: 10.1111/j.1151-2916.2003.tb03481.x

Garcia-Lodeiro, I., Palomo, A., Fernández-Jiménez, A., and Macphee, D. (2011). Compatibility studies between NASH and CASH gels. Study in the ternary diagram Na2O–CaO–Al2O3–SiO2– H2O. *Cement Concrete Res.* 41, 923–931. doi: 10.1016/j.cemconres.2011.05.006

Häkkinen, T. (1993). The influence of slag content on the microstructure, permeability and mechanical properties of concrete part 1 microstructural studies and basic mechanical properties. *Cement Concrete Res.* 23, 407–421. doi: 10.1016/0008-8846(93)90106-J

Helmuth, G. J., and Verbeck, R. A. (1968). "Structures and physical properties of cement paste," in *Proceedings of the 5th International Symposium on the Chemistry of Cement* (Tokyo).

Higgins, D. (1982). *Efflorescence on Concrete.* Slough: Cement and Concrete Association.

Humad, A. M., Kothari, A., Provis, J. L., and Cwirzen, A. (2019). The effect of blast furnace slag/fly ash ratio on setting, strength, and shrinkage of alkali-activated pastes and concretes. *Front. Mater.* 6:9. doi: 10.3389/fmats.2019.00009

Humad, A. M., Provis, J. L., and Cwirzen, A. (2018). Alkali activation of a high MgO GGBS–fresh and hardened properties. *Mag. Concrete Res.* 70, 1256–1264. doi: 10.1680/jmacr.17.00436

Ismail, I., Bernal, S. A., Provis, J., Hamdan, S., and Van Deventer, J. S. J. (2013). Drying-induced changes in the structure of Alkali-activated pastes. *J. Mater. Sci.* 48, 3566–3577. doi: 10.1007/s10853-013-7152-9

Jiang, W., Silsbee, M., Breval, E., and Roy, D. (1997). "Alkali-activated cementitious materials in chemically aggressive environments," in *Mechanisms of Chemically Degradation of Cement-Based Systems.E&FN SPON* (Gothenburg-Sweden), 289–296.

Karahan, O., and Yakupoglu, A. (2011). Resistance of alkali-activated slag mortar to abrasion and fire. *Adv. Cement Res.* 23, 289–297. doi: 10.1680/adcr.2011.23.6.289

Krizan, D., and Zivanovic, B. (2002). Effects of dosage and modulus of water glass on early hydration of alkali–slag cements. *Cement Concrete Res.* 32, 1181–1188. doi: 10.1016/S0008-8846(01)00717-7

Lloyd, R. R., Provis, J. L., and Van Deventer, J. S. (2010). Pore solution composition and alkali diffusion in inorganic polymer cement. *Cement Concrete Res.* 40, 1386–1392. doi: 10.1016/j.cemconres.2010.04.008

Longhi, M. A., Zhang, Z., Rodríguez, E. D., Kirchheim, A. P., and Wang, H. (2019). Efflorescence of Alkali-activated cements (geopolymers) and the impacts on material structures: a critical analysis. *Front. Mater.* 6:89. doi: 10.3389/fmats.2019.00089

Ma, J., and Dehn, F. (2017). Shrinkage and creep behavior of an alkali-activated slag concrete. *Struct. Concrete* 18, 801–810. doi: 10.1002/suco.201600147

Mosale Vijayakumar, R. (2014). *Evaluating Shrinkage of Fly Ash - Slag Geopolymers*. University of Illinois at Urbana-Champaign. Available online at: http://hdl.handle.net/2142/46792

Mundra, S., Bernal Lopez, S., Criado, M., Hlavácek, P., Ebell, G., Reinemann, S., et al. (2017). Steel corrosion in reinforced alkali-activated materials. *RILEM Tech. Lett.* 2, 33–39. doi: 10.21809/rilemtechlett.2017.39

Myers, R. J., Bernal, S. A., and Provis, J. L. (2017). Phase diagrams for alkali-activated slag binders. *Cement Concrete Res.* 95, 30–38. doi: 10.1016/j.cemconres.2017.02.006

Neto, A. A. M., Cincotto, M. A., and Repette, W. (2008). Drying and autogenous shrinkage of pastes and mortars with activated slag cement. *Cement Concrete Res.* 38, 565–574. doi: 10.1016/j.cemconres.2007.11.002

Orosz, K., Humad, A., Hedlund, H., and Cwirzen, A. (2019). Autogenous deformation of Alkali-activated blast furnace slag concrete subjected to variable curing temperatures. *Adv. Civil Eng.* 2019:8. doi: 10.1155/2019/6903725

Palacios, M., and Puertas, F. (2007). Effect of shrinkage-reducing admixtures on the properties of alkali-activated slag mortars and pastes. *Cement Concrete Res.* 37, 691–702. doi: 10.1016/j.cemconres.2006.11.021

Park, S. M., Jang, J. G., and Lee, H. K. (2018). Unlocking the role of MgO in the carbonation of alkali-activated slag cement. *Inorg. Chem. Front.* 5, 1661–1670. doi: 10.1039/c7qi00754j

Provis, J. L., Palomo, A., and Shi, C. (2015) Advances in understanding alkali-activated materials. *Cement Concrete Res.* 78, 110–125. doi: 10.1016/j.cemconres.2015.04.013

Provis, J. L., and Van Deventer, J. S. (2014). *Alkali Activated Materials.* London: Springer.

Sariibrahimoglu, K., Leeuwenburgh, S. C., Wolke, J. G., Yubao, L., and Jansen, J. A. (2012). Effect of calcium carbonate on hardening, physicochemical properties, and *in vitro* degradation of injectable calcium phosphate cements. *J. Biomed. Mater. Res. Part A* 100, 712–719. doi: 10.1002/jbm.a.34009

Shi, C. (1996). Strength, pore structure and permeability of alkali-activated slag mortars. *Cement Concrete Res.* 26, 1789–1799. doi: 10.1016/S0008-8846(96)00174-3

Shi, C., and Day, R. L. (1996). Some factors affecting early hydration of alkali-slag cements. *Cement Concrete Res.* 26, 439–447. doi: 10.1016/S0008-8846(96)85031-9

Shi, C., Krivenko, P. V., and Roy, D. (2006) *Alkali-Activated Cements and Concretes*. London: CRC Press. doi: 10.4324/9780203390672

Singh, B., Rahman, M., Paswan, R., and Bhattacharyya, S. (2016). Effect of activator concentration on the strength, ITZ and drying shrinkage of fly ash/slag geopolymer concrete. *Constr. Build. Mater.* 118, 171–179. doi: 10.1016/j.conbuildmat.2016.05.008

Van Deventer, J., Nicolas, R. S., Ismail, I., Bernal, S., Brice, D., and Provis, J. (2014). Microstructure and durability of alkali-activated materials as key parameters for standardization. *J. Sustain. Cement Based Mater.* 4, 116–128. doi: 10.1080/21650373.2014.979265

Wallah, S., and Rangan, B. V. (2006). *Low-Calcium Fly Ash-Based Geopolymer Concrete: Long-Term Properties*. Curtin University of Technology.

Wang, S., Pu, X., Scrivener, K., and Pratt, P. (1995). Alkali-activated slag cement and concrete: a review of properties and problems. *Adv. Cement Res.* 7, 93–102. doi: 10.1680/adcr.1995.7.27.93

Wedatalla, A. M. O., Jia, Y., and Ahmed, A. A. M. (2019). Curing effects on high-strength concrete properties. *Adv. Civil Eng.* 2019:1683292. doi: 10.1155/2019/1683292

Xu, H., Provis, J. L., van Deventer, J. S., and Krivenko, P. V. (2008). Characterization of aged slag concretes. *ACI Mater. J.* 105, 131. doi: 10.14359/19753

Yang, K., Song, J., and Song, K. (2013). Assessment of CO2 reduction of alkali-activated concrete. *J. Clean. Prod.* 39, 265–272. doi: 10.1016/j.jclepro.2012.08.001

Ye, H., Cartwright, C., Rajabipour, F., and Radlinska, A. (2017). Understanding the drying shrinkage performance of alkali-activated slag mortars. *Cement Concrete Composites* 76, 13–24. doi: 10.1016/j.cemconcomp.2016.11.010

Ye, H., and Radlinska, A. (2016). Quantitative analysis of phase assemblage and chemical shrinkage of alkali-activated slag. *J. Adv. Concrete Technol.* 14, 245–260. doi: 10.3151/jact.14.245

Zhang, W., Zakaria, M., and Hama, Y. (2013). Influence of aggregate materials characteristics on the drying shrinkage properties of mortar and concrete. *Constr. Build. Mater.* 49, 500–510. doi: 10.1016/j.conbuildmat.2013.08.069

Zheng, Y. C. (2010). *Shrinkage Behaviour of Geopolymers*. The University of Melbourne. Available online at: https://minerva-access.unimelb.edu.au/handle/11343/35358

Conflict of Interest: The authors declare that the research was conducted in the absence of any commercial or financial relationships that could be construed as a potential conflict of interest.